ACTIVE CONTROL OF AN AXISYMMETRIC JET WITH AN INTELLIGENT NOZZLE

Hiroaki Suzuki

Nobuhide Kasagi

Yuji Suzuki

Department of Mechanical Engineering, The University of Tokyo
Hongo, Bunkyo-ku, Tokyo 113-8656, Japan

ABSTRACT

An intelligent nozzle equipped with a row of miniature flap actuators on its exit lip is developed for active flow control. The spatio-temporal structures of the controlled jet are studied through two-dimensional velocity field measurement. When each half cluster of flaps are driven out of phase, the jet clearly bifurcates into two branches. The detailed bifurcating mechanism is explored by examining phase-averaged velocity and vorticity fields. It is found that the vortex ring, which is alternatively inclined due to the difference of induced velocities between the upper and lower halves, causes the stable slip-through motion with the preceding half of vortex ring. This interaction makes each half of vortex ring turn away from the jet axis. These strongly inclined vortex rings vectorize the jet core fluid alternatively, and thus results in the bifurcating jet.

INTRODUCTION

Controlling turbulent shear flows and associated scalar transport in various engineering applications and the environment should lead to significant benefits for the welfare of human being. The characteristics of turbulent flows, e.g., drag, flow induced noise, heat transfer, and mixing, are ruled by coherent structures arising in each shear flow (Cantwell, 1981). The scales of these structures, however, are usually very small, and their lifetime is also very short. In the past, direct manipulation of these scales was impractical, but now expected to become possible with miniature sensors and actuators fabricated by MEMS (Microelectromechanical Systems) (Ho & Tai, 1996). In addition, micromechanical components will possibly be produced in large quantities through a batch production process. Therefore, active and direct flow control by using distributed miniature devices has become a realistic technological target.

Among various turbulent shear flows, jets are used in a variety of industrial applications, such as mixing, heating/cooling, drying, spraying, printing, and thrusting. In this particular flow mode, large-scale coherent structures emerge from initial small disturbances through inherent amplification mechanism. When a jet flow is excited by periodic acoustic forcing, which superimposes an oscillating component on the uniform exit velocity, strong organized vortices play a primary role in momentum and scalar transport (Zaman & Hussain, 1980). Thus, it is expected that large alteration in the downstream flow field could be achieved with a relatively small control input. In the recent studies, some sophisticated controls are demonstrated. Lee & Reynolds (1985) found that a jet flow can be forced to bloom or bifurcate by a combined effect of a precessing nozzle and axial forcing. Huang et al. (1996) developed an axisymmetric jet nozzle equipped with electrostatic micro actuators to suppress the screech in a high speed jet.

Previously, Suzuki et al. (1999) developed an "intelligent" nozzle, equipped with a row of miniature flap actuators on its axisymmetric nozzle lip, and investigated the response of jet to various control modes by using flow visualization. The objective of the present study is to explore the dynamics of coherent vortical structures of the jet controlled by the intelligent nozzle, and its contribution to the global flow evolution. To do this, spatio-temporal velocity and vorticity fields are examined by using two-dimensional particle tracking velocimetry (2-D PTV).

EXPERIMENTAL FACILITY AND TECHNIQUES

Figure 1 shows a perspective view of an intelligent nozzle (diameter D = 20 mm) equipped with 18 electromagnetic flap actuators. Each flap actuator, 9 mm in length and 3 mm in width, is made of 25 μm-thick polyimide film, on which a 35 μm-thick copper square coil is photofabricated by ferric chloride etching. They are elastically bent by the electromagnetic force between the copper coil and a cylindrical permanent

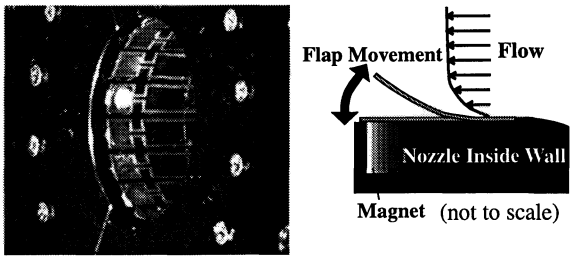

Fig. 1 (a) Intelligent nozzle, (b) Flap movement.

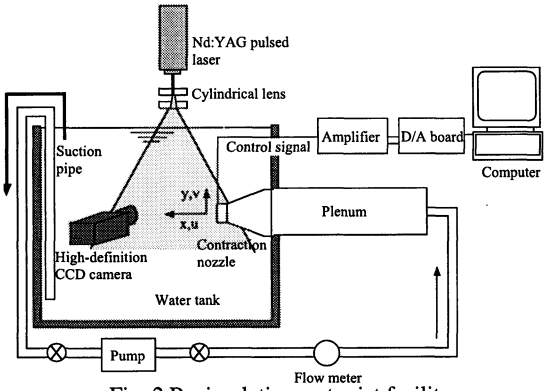

Fig. 2 Recirculating water jet facility.

magnet embedded underneath. These flaps placed inside the nozzle exit at regular intervals cover 86% of the circumference. Each flap is independently driven by the amplified electric current from a multi-channel digital-analog board. The amplitude of the flap is 0.4 mm, which is almost the same as the initial shear layer thickness in the present study.

A schematic of the recirculating water test facility and the coordinate system is shown in Fig. 2. The jet nozzle and a plenum are connected to the water tank ($900 \times 800 \times 800$ mm^3) horizontally. The Cartesian coordinate system is employed, where x denotes the streamwise direction, while y and z are the two perpendicular (vertical and horizontal) radial directions, respectively. Water is driven by a magnetic pump through a honeycomb and meshes in the 130 mm ID plenum in order to reduce the fluctuation and obtain a uniform mean flow distribution at the nozzle exit. The nozzle has an area contraction ratio of 42 : 1 and a wall profile fit to a third-order polynomial.

For flow visualization of jet shear layer, a fluorescent dye (Rhodamine B) solution is injected from an annular slot assembled inside the nozzle. A two-component fiber LDV (DANTEC 60X11) is employed to measure jet centerline velocity for spectrum analysis.

Spatio-temporal evolution of large-scale vortical structures is investigated by using 2-D PTV. The particle images are acquired by using a high definition CCD camera (Sony XCH-1125; 1920×1024 pixel^2) through a circular window on the side wall of the tank, and recorded onto a laser disk recorder (Sony HDL-5800) at 30 frame/s. A light sheet of about 1 mm in thickness is formed with Nd:YAG laser (Newwave Research Minilase II), and introduced vertically into the flow field. The frequency of the laser pulse is set at 60 Hz, so that particles are captured on successive field images at a 1/60s time interval. Flap driving signal and the laser pulse are synchronized with the TV signal. An analog image preprocessor (Nexus VP-01) is employed to improve the signal-to-noise (S/N) ratio of particle images. The acquired images are A/D converted by an image processor (Nexus 9000) and transferred to a workstation. Instantaneous velocity vectors are obtained by tracking each particle over three consecutive time steps. A binary cross-correlation method (Yamamoto et al., 1991) is employed to reject spurious vectors.

The flow is seeded with Nylon 12 spherical particles having a specific gravity of 1.02 and a diameter ranging between 140 and 170 μm. The seeding concentration is 1.5×10^{-4} g/cm^3. The measurement area is 110×60 mm^2 ($5.5D \times 3D$). Statistics are calculated as ensemble averages using 5600 instantaneous velocity fields in each sub-region of 1.56×1.56 mm^2 (76×40 cells).

The jet centerline exit velocity U_0 is set to be 151 mm/s, corresponding to $Re_D = 3000$ throughout the present measurement.

RESULTS

Excitation characteristics by flap actuators

Figure 3 shows a longitudinal sectional view of the jet controlled by axisymmetric flap motion, in which all 18 flaps are driven in phase with by a square wave signal of $f_a = 4$ Hz ($St_a = f_aD/U_0 = 0.53$). It can be observed that organized axisymmetric vortex rings synchronized with the flap movement frequency are shed with a regular spacing. The rms streamwise velocity fluctuation at $x/D = 0.25$ in the excited jet is $0.026U_0$ and $0.22U_0$ at the centerline and in the shear layer, respectively. In the natural jet, it is $0.022U_0$ and $0.13U_0$, respectively. Therefore, unlike acoustic forcing, the disturbance presently generated by the flaps is introduced locally in the shear layer.

Figure 4 shows one-dimensional spectra of the centerline streamwise velocity at $x/D = 3$ with various flapping frequencies of the axisymmetric mode. The spectra show sharp peaks at the fundamental frequency ($f/f_a = 1$), when $St_a = 0.3 \sim 0.5$. These peaks indicate the vortex ring generation locked-in with the flap movement and the vortex pairing is suppressed. This phenomenon corresponds to the preferred mode found by Crow & Champagne (1971). At higher St_a (> 0.6), the fundamental peak disappears as a weak subharmonic peak appears, which indicate that the stable vortex pairing occurs near the nozzle exit. Existence of the second harmonic peak ($f/f_a = 2$) at

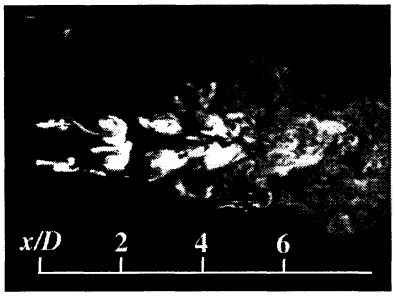

Fig. 3 Axisymmetric structures locked-in with synchronous flap movement at $St_a = 0.53$.

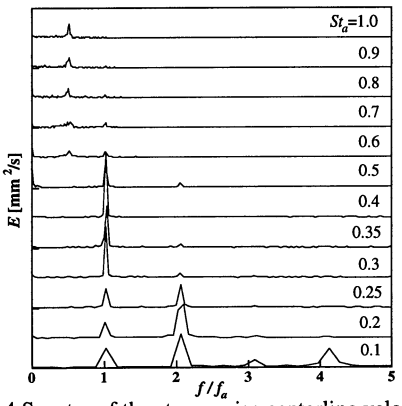

Fig. 4 Spectra of the streamwise centerline velocity at various flapping frequency.

lower St_a (0.1 ~ 0.25) implies that two vortex rings are shed during one cycle of the flap movement; vortex rings are shed with both ascending and descending motions of the flaps.

Statistics of the controlled jets

Suzuki et al. (1999) show that, when each half cluster of the flaps are driven 180-degree out of phase (alternative mode; hereafter referred as AM), the jet bifurcates into two separate jets from x/D = 3. To clarify the relevant conditions of flapping Strauhal number St_a and Re_D for the jet bifurcation with AM, the centerline velocity at x/D = 6 is measured by LDV. Figure 5 shows the contours of the mean centerline velocity normalized by that of the natural jet at the same Re_D. The centerline velocity is decelerated to as much as 40-50% with the optimum flapping frequency of St_a = 0.25. The reduction rate is insensitive to Re_D under the present experimental condition at Re_D = 1800 ~ 13000.

The jets tested and the conditions of 2-D PTV measurement are summarized in Table 1. For the bifurcating jet with AM, the measurement is made in two perpendicular planes, i.e., in the plane of bifurcation (bifurcating plane) and out of the plane (bisecting plane). These planes include the y and z directions, respectively.

Figures 6 (a) and (b) show phase-averaged velocity fields of the AM controlled jet at St_a = 0.25 in the bifurcating and bisecting planes. The definition of the ensemble- (phase-) average of any instantaneous flow variable f at a specific phase ϕ is given by

$$< f(\boldsymbol{x},\phi) >= \frac{1}{N}\sum_{n=1}^{N} f\left(\boldsymbol{x}, \frac{T}{2\pi}(\phi + 2\pi n)\right), \qquad (1)$$

where T is the actuation period. Alternatively flipped jet core can be seen clearly in the bifurcating plane. On the other hand, the jet fluid momentum decays and ambient fluid moves toward the jet centerline at x/D = 3 ~ 4 in the bisecting plane.

Figure 7 shows the cross-stream distributions of the streamwise mean velocity U at various axial locations. The velocity profiles near the nozzle exit (x/D = 0.5) are almost the same in all cases. At x/D = 3, which corresponds to the bifurcating point, the centerline velocity of the bifurcating jet is decreased than that of the natural jet. The profile becomes wider in the bifurcating plane, while the width of the jet is

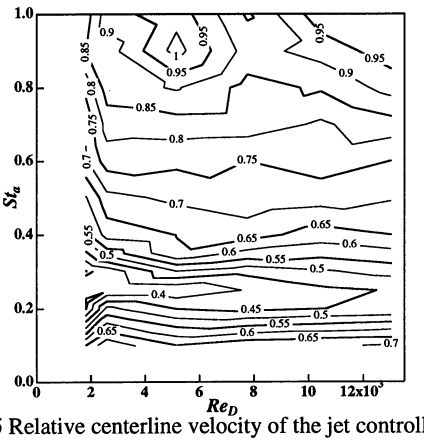

Fig. 5 Relative centerline velocity of the jet controlled at various flapping frequency.

Table 1. Experimental conditions.

Control Mode	Flap Motion Strauhal Number (St_a)
Natural Jet	-
Alternative Mode (Bifurcating Plane)	0.125, 0.25(optimum), 0.5
Alternative Mode (Bisecting Plane)	0.25 (optimum)
Axisymmetric Mode	0.3 (preferred mode)

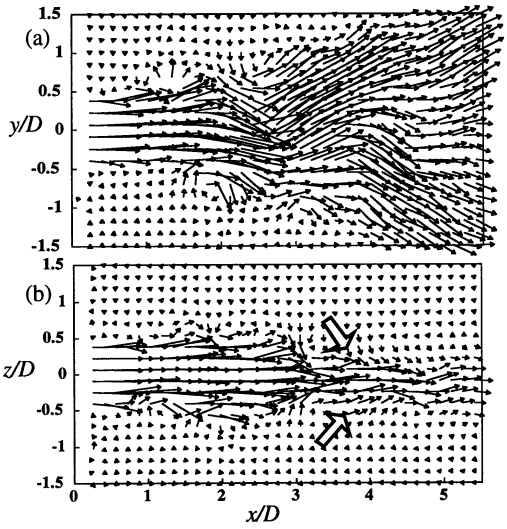

Fig. 6 Phase-averaed velocity fields of the AM controlled jet; (a) bifurcating plane, (b) bisecting plane.

reduced in the bisecting plane. At x/D =5, the profile exhibits two separate peaks and a trough at the centerline in the bifurcating plane.

Figure 8 shows the streamwise distributions of the mean velocity U. For the natural jet, U remains unchanged up to x/D = 4, thus the potential core should persist in this region. On the other hand, U is decreased rapidly from x/D = 2 in the AM controlled jet; with St_a = 0.25, U at x/D = 5.5 is reduced to as low as $0.3U_0$, while $0.6U_0$ and $0.5U_0$ when St_a = 0.125 and 0.5, respectively. It is separately confirmed that, in the

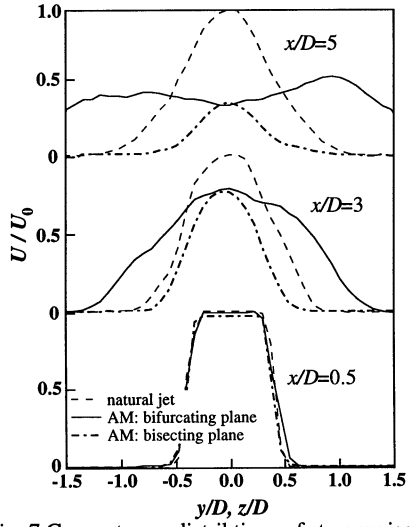

Fig. 7 Cross-stream distribtions of streamwise mean velocities.

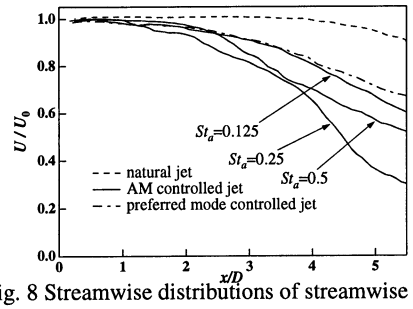

Fig. 8 Streamwise distributions of streamwise mean velocities.

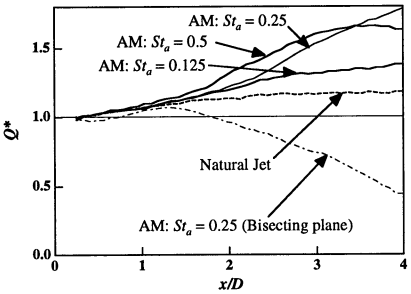

Fig. 9 Streamwise distributions of relative volume flux.

axisymmetric-mode control, the jet velocity is also dropped. It is, however, mainly because the amplified vortex rings entrain more stationary ambient fluid into the jet core.

The entrainment of the jet can be evaluated by the volume flux of the mean velocity field. The relative volume flux $Q^*(x)$ in a 2-D plane defined by:

$$Q^*(x) = \int_{-\infty}^{\infty} U(x,y)/U_0 dy, \text{ or, } = \int_{-\infty}^{\infty} U(x,z)/U_0 dz \quad (2)$$

is shown in Fig. 9. In the natural jet, Q^* is slightly increased and becomes 1.2 at x/D =4. For the AM controlled jet, Q^* in the bifurcating plane is markedly increased at $x/D > 1.5$ and reaches 1.4, 1.8, and 1.6 for $St_a = 0.125$, 0.25, and 0.5, respectively. Note that Q^* for $St_a = 0.5$ is the largest at $x/D < 3.2$, although Q^* for $St_a = 0.25$ becomes larger in the further downstream region. On the other hand, Q^* in the bisecting plane is decreased at $x/D > 1.5$.

Bifurcating mechanism in alternative mode control

Figures 10 (a)~(d) show the successive flow visualization images of the AM controlled jet at $St_a = 0.25$. When $\phi = 0$, the flaps located on the lower half of the jet nozzle are ascending toward the jet centerline in Fig. 10 (a), while those on the upper half are descending toward the nozzle-inside wall. Two relatively large blobs of dye are seen right downstream the nozzle exit, but no vortex can be identified. When $\phi = 0.27\pi$, a vortex labeled A rolls up in the lower half of the nozzle (Fig. 10 b). On the other hand, the roll-up in the upper half is delayed, and another vortex appears at 0.54π (vortex labeled B, Fig. 10 c). Therefore, the vortex ring formed in AM control is initially inclined with respect to the nozzle axis. The convective velocity of vortex A is larger than that of vortex B, and the ratio is about 1.7 at $x/D = 0.9$. Thus, the vortex ring is further inclined and bent as it is convected downstream as shown in Fig. 10 (d).

Figures 11 (a)~(d) show phase-averaged vorticity contour diagrams. The phase difference of the diagrams is $\pi/2$. A pair of circles and a connecting line represent a vortex ring, which has been identified in the flow visualization image. The value of vorticity $<\omega_z>$ is normalized with U_0 and D. As has been shown in Fig. 10, an inclined vortex ring rolls up at $x/D \sim 1$. In Fig. 11 (a), the upper half (B) generated by the flap descending motion has larger vorticity (denoted as a larger circle) than the lower half (A) generated by the flap ascending motion (denoted as a smaller circle). Thus, the difference of convective velocity between the upper and lower halves mentioned previously can be attributed to the asymmetric vorticity distribution along the vortex ring; i.e., the upper half having larger circulation induces larger convective velocity at the lower half.

Accordingly, the lower half (A) goes ahead of the upper half (B), and overtakes the lower half of the preceding vortex

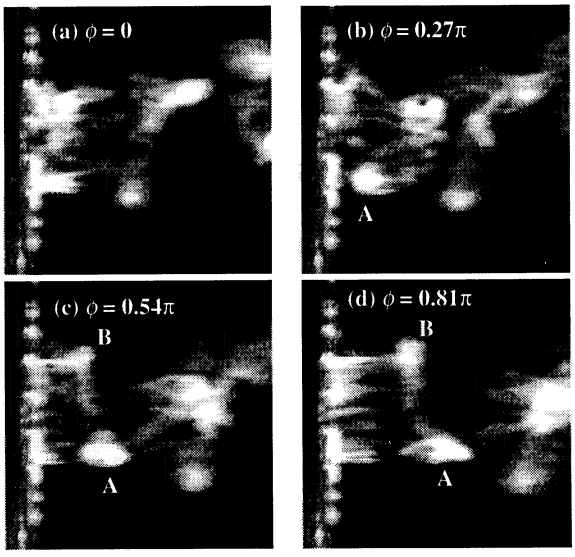

Fig. 10 Successive flow visualization images near the nozzle exit of the AM controlled jet.

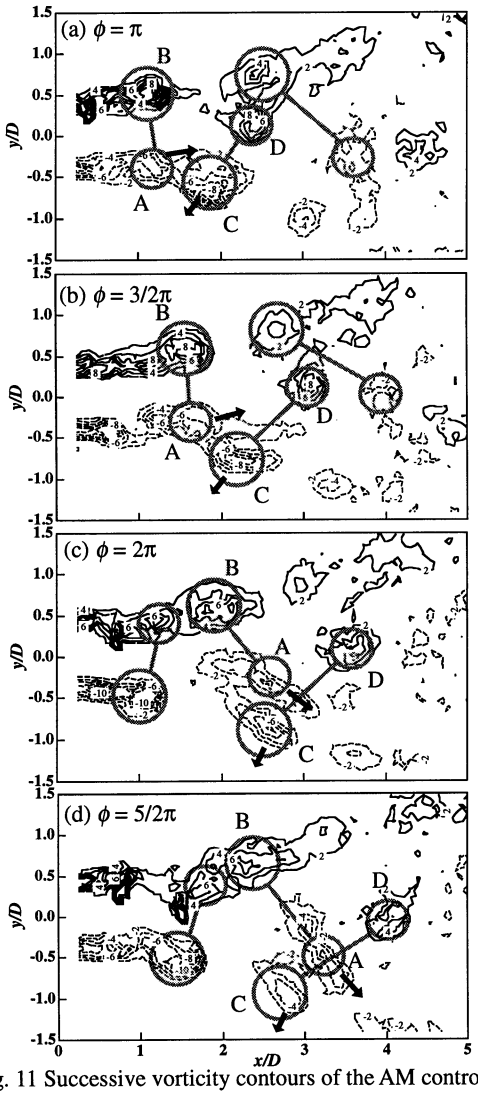

Fig. 11 Successive vorticity contours of the AM controlled jet at $St_a = 0.25$.

ring (C) having larger circulation as shown in Fig. 11 (b). Then, by the action of mutual interaction, vortex C is displaced outward and decelerated, while vortex A moves inward and is accelerated (Fig. 11 b, c). As the interaction proceeds, vortex A slips through the vortex ring C-D, and moves toward the off-axis direction. This alternative slip-through phenomenon is accomplished at around $x/D = 3$, and these vortical structures gradually dissipate further downstream.

Figure 12 shows the phase-averaged velocity vectors, on which the vorticity magnitude of $|<\omega_z>|D/U_0 > 3.5$ at corresponding phase is superimposed. The jet core fluid inside the inclined vortex rings is alternatively vectorized away from the jet axis, causing alternative flipping of the fluid.

To examine the behavior of jet potential core at different flapping frequency, the regions of velocity magnitude $< U_{abs} > \left(\equiv \sqrt{< u >^2 + < v >^2} \right) > 0.85 U_0$ are shown along with vorticity contours in Fig. 13. At the optimum flapping

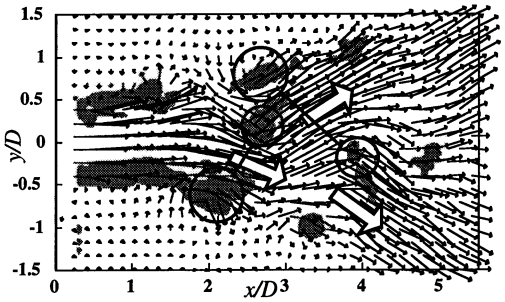

Fig. 12 Phase-averaged velocity field with a vorticity magnitude (shaded area) at $St_a = 0.25$.

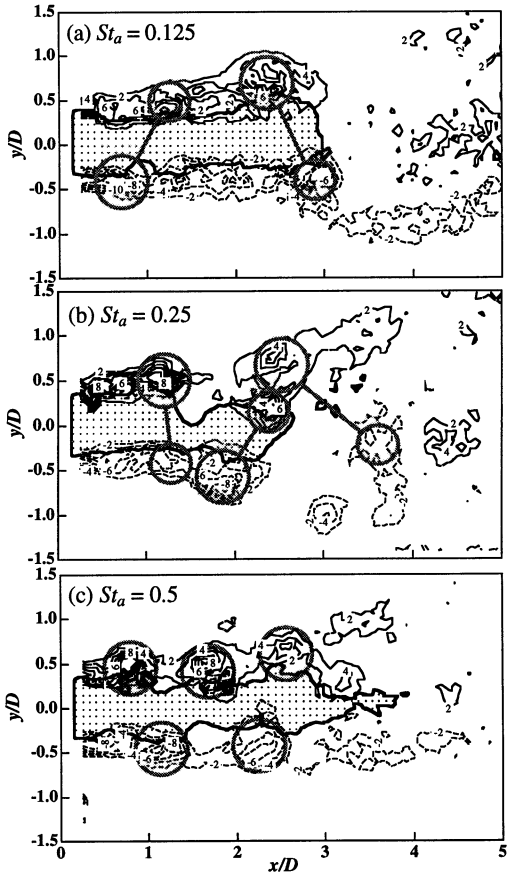

Fig. 13 Jet potential core (shaded area) and vorticity contours.

frequency of $St_a = 0.25$, the potential core oscillates in the cross-stream direction vigorously. The constriction between the neighboring vortices indicates that the stationary ambient fluid is entrained toward the centerline. At the lower St_a (= 0.125, Fig. 11 a), however, the slip-through interaction between alternatively inclined vortex rings does not occur, since the spacing of the successive vortex rings is much larger. Therefore, jet core oscillates less vigorously. At the higher St_a (= 0.5, Fig. 11 c), the spacing of the successive vortex rings is very small, so that the half vortex having smaller circulation mentioned before must have been engulfed by the half vortex with larger circulation in the vicinity of the exit nozzle. Hence, the strong

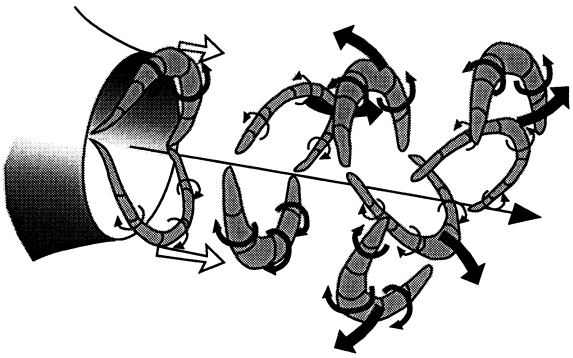

Fig. 14 Schematic diagram of vortex structures of the bifurcating jet.

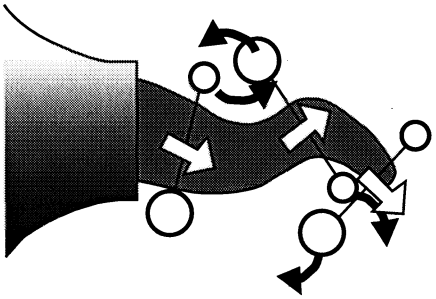

Fig. 15 Schematic diagram of jet core oscillation of the bifurcating jet.

vortices generated by the flap descent line up in a staggered arrangement at a regular spacing, and only small undulation of the potential core with short interval exists. However, the slip-through phenomenon also does not occur, because the convective velocities of the neighboring vortices are not much different.

A scenario of the vortex motion in the bifurcating jet derived from the present results is schematically given in Fig. 14. With the out-of-phase flapping of each half cluster of the flaps, a vortex ring with different magnitude of circulation between upper and lower halves rolls up; the stronger half is generated by the flap descending, and the weaker half is generated by the flap ascending. The stronger half induces larger convective velocity on the weaker half, so that the weaker half travels faster than the stronger half. As the weaker half approaches the stronger half of the preceding vortex ring, the weaker half slips through the preceding vortex ring. Then, by the mutual interaction, both are directed toward the off-axis directions.

Figure 15 shows a schematic diagram of jet core oscillation in the bifurcating jet. In consequence of the vortex interaction mentioned above, the vortex rings are strongly inclined, and they induce the alternative off-axis velocity to the jet core fluid.

In the bifurcating jet of Lee & Reynolds (1985), the jet separates into two branches at $x/D = 5 \sim 6$ due to the mutual interaction of slightly tilting vortex rings, which are convected without pairing. In the present control, the difference in convective velocity between the upper and lower halves of a vortex ring causes strong interaction between vortices. Thus, the jet bifurcates at a shorter streamwise distance.

CONCLUDING REMARKS

An novel axisymmetric jet nozzle equipped with a row of miniature electromagnetic flap actuators on its exit lip has been developed. The behavior of the controlled jet flow is examined through flow visualization and 2-D PTV velocity measurement. When each half cluster of the flaps are driven 180-degree out of phase (alternative mode), the jet bifurcates into two separate jets without any bulk flow forcing. The optimum flapping Strauhal number is $St_a = 0.25$ for $Re_D < 13000$. It is found that alternatively inclined and bent vortex rings are formed near the nozzle exit. As they are convected downstream, they induce stable slip-through motion and turn away from the original jet axis. On the basis of the present results, an conceptual model of the bifurcating jet is presented. It is suggested that the difference of circulation between the upper and lower halves of the vortex ring and their convective velocities should be responsible for the jet bifurcation.

ACKNOWLEDGEMENT

The authors gratefully acknowledge Professors H. Miura and I. Shimoyama for their guidance in developing the actuators. This work was supported by Ministry of Education, Science, Culture and Sports through the Grant-in-Aid for Scientific Research (No. 10355010).

REFERENCES

Cantwell, B. J., 1981, "Organized Motion in Turbulent Flow," *Ann. Rev. Fluid Mech.*, Vol. 13, pp. 437-515.

Crow, S. C., and Champagne, F. H., 1971, "Orderly Structure in jet turbulence," *J. Fluid Mech.*, Vol. 48, pp. 547-591.

Ho, C.-M., and Tai, Y.-C., 1996, "Review: MEMS and Its Applications for Flow Control," *ASME J. Fluids Eng.*, Vol. 118, pp. 437-447.

Huang, C., et al., 1996, "A Microactuator System for the Study and Control of Screech in High Speed Jets," *IEEE MEMS Workshop Proceedings*, San Diego, pp. 19-24.

Lee, M., and Reynolds, W. C., 1985, "Bifurcating and Blooming Jets," *Report TF-22, Thermosciences Division, Dept. of Mech. Eng., Stanford University.*

Suzuki, H., et al., 1999, "Manipulation of a Round Jet with Electromagnetic Flap Actuators," *IEEE MEMS Conference Proceedings*, Orlando, pp. 534-540.

Yamamoto, F., et al., 1991, "A Binary Correlation Method Using a Proximity Function for 2-D and 3-D PTV," *Exp. Numerical Flow Vis.*, Khalighi, B., et al., eds., New York, ASME, pp. 23-28.

Zaman, K. B. M. Q., and Hussain, A. K. M. F., 1980, "Vortex Pairing in a Circular Jet Under Controlled Excitation. Part 1. General Jet Response," *J. Fluid Mech.*, Vol. 101, pp.449-491.